

# The Batch Artifact Scanning Protocol: A new method using computed tomography (CT) to rapidly create three-dimensional models of objects from large collections *en masse*\*

Katrina Yezzi-Woodley<sup>†</sup>    Jeff Calder<sup>‡</sup>    Mckenzie Sweno<sup>§</sup>  
 Chloe Siewert<sup>§</sup>    Peter J. Olver<sup>‡</sup>

## Abstract

Within anthropology, the use of three-dimensional (3D) imaging has become increasingly standard and widespread since it broadens the available avenues for addressing a wide range of key issues. The ease with which 3D models can be shared has had major impacts for research, cultural heritage, education, science communication, and public engagement, as well as contributing to the preservation of the physical specimens and archiving collections in widely accessible data bases. Current scanning protocols have the ability to create the required research quality 3D models; however, they tend to be time and labor intensive and not practical when working with large collections. Here we describe a streamlined, *Batch Artifact Scanning Protocol* we have developed to rapidly create 3D models using a medical CT scanner. Though this method can be used on a variety of material types, we use a large collection of experimentally broken ungulate limb bones. Using the Batch Artifact Scanning Protocol, we were able to efficiently create 3D models of 2,474 bone fragments at a rate of less than 3 minutes per specimen, as opposed to an average of 50 minutes per specimen using structured light scanning.

**Keywords**— computed tomography, scanning, 3D models, bone fragments

## 1 Introduction

The use of 3D imaging within anthropology is surging in popularity because it expands, in astounding ways, the avenues used for addressing anthropological questions, (Frischer & Dakouri-Hild, 2008; Hirst, White, & Smith, 2018; Mafart, Guipert, De Lumley, & Subsol, 2004; Remondino & Campana, 2014; Uldin, 2017; Weber & Bookstein, 2011). For example, researchers are able to reassemble fragmentary objects,

---

\*Source Code: <https://github.com/jwcalder/CT-Surfacing>

<sup>†</sup>Department of Anthropology, University of Minnesota, yezz0003@umn.edu (corresponding author)

<sup>‡</sup>School of Mathematics, University of Minnesota

<sup>§</sup>Department of Anthropology, University of Minnesota

reconstruct missing structures, mitigate taphonomic distortion (e.g. Amano et al., 2015; Benazzi, Bookstein, Strait, & Weber, 2011; Benazzi, Gruppioni, Strait, & Hublin, 2014; Benazzi, Orlandi, & Gruppioni, 2009; Berger et al., 2015; Bermúdez de Castro et al., 2016; Delpiano, Peresani, & Pastoors, 2017; Gunz, Mitteroecker, Neubauer, Weber, & Bookstein, 2009; Kikuchi & Ogihara, 2013; Lovejoy, Suwa, Spurlock, Asfaw, & White, 2009; Papaioannou & Karabassi, 2003; Papaioannou, Karabassi, & Theoharis, 2001, 2002; Pletinckx, 2011; Ponce De León, 2002; Ponce De León & Zollikofer, 1999; Tobias, 2001; C. P. Zollikofer et al., 2005; C. P. Zollikofer, de León, Martin, & Stucki, 1995; C. P. E. Zollikofer, Ponce De León, & Martin, 1998; Zvietcovich, Navarro, Saldana, Castillo, & Castaneda, 2016), advance geometric morphometric research (e.g. Baab, McNulty, & Harvati, 2013; Baab, McNulty, & Rohlf, 2012; Bastir et al., 2019; Jani, Johnson, Parekh, Thompson, & Pandey, 2020; Knigge et al., 2021; Knigge, Tocheri, Orr, & McNulty, 2015; Knyaz & Gaboutchian, 2021; McNulty, 2005; White, Pope, Hillson, & Soligo, 2022), improve upon the ways in which data are collected, and to extract new types of data that cannot be collected directly from the object (e.g. Baab et al., 2012; O'Neill et al., 2020; Pante et al., 2017; Schulz-Kornas, Kaiser, Calandra, & Winkler, 2020; Yezzi-Woodley et al., 2021, just to name a few). And, in the case of computed-tomography (CT) it can be leveraged to non-destructively access otherwise inaccessible internal structures (e.g. the neurocranium, endocranium, or pneumatization and sinuses) (Ponce De León & Zollikofer, 1999; Seidler et al., 1997; Tobias, 2001; Wu & Schepartz, 2009), virtually differentiate fossils from adhering matrix or infilled cavities (Bräuer et al., 2004; Conroy & Vannier, 1984; Tobias, 2001; C. P. E. Zollikofer et al., 1998), or even view mummies inside their encasements (White, Hirst, & Smith, 2018; Wu & Schepartz, 2009). 3D models have been used for studies on biomechanics (O'Higgins et al., 2011; Spoor, Wood, & Zonneveld, 1994; Strait et al., 2009; Weber, 2014; Weber, Bookstein, & Strait, 2011) and allometry and ontogeny (Massey, 2018; Penin, Berge, & Baylac, 2002; Ponce de León & Zollikofer, 2001). For objects where 2D sketches are used widely, such as stone tools and pottery, 3D models have been used to create 2D technical drawings in a more time efficient, consistent, and reliable manner (e.g. Barone, Neri, Paoli, & Razionale, 2018; Hörr, 2009; Magnani, 2014). 3D models have been used to refine typologies (Grosman, Smikt, & Smilansky, 2008) and analyze reduction and operational sequences (Clarkson, 2013; Clarkson, Shipton, & Weisler, 2014; Hermon, Polig, Driessen, Jans, & Bretschneider, 2018). Zooarchaeologists and taphonomists are using 3D models generated via micro-CT, micro-photogrammetry, structured light scanning, and high power imaging microscopes to study bone surface modifications and surface texture (Aramendi et al., 2017; Arriaza et al., 2019, 2017; Bello, 2011; Bello, Parfitt, & Stringer, 2009; Bello & Soligo, 2008; Boschini & Crezzini, 2012; Boschini, Zanolli, Bernardini, Princivalle, & Tuniz, 2015; Courtenay, Yravedra, Huguet, et al., 2019; Courtenay, Yravedra, Mate-González, Aramendi, & González-Aguilera, 2019; González, Yravedra, González-Aguilera, Palomeque-González, & Domínguez-Rodrigo, 2015; Gümrükçü & Pante, 2018; López-Cisneros et al., 2019; Martisius, McPherron, Schulz-Kornas, Soressi, & Steele, 2020; Maté-González et al., 2017; Maté-González, Courtenay, et al., 2019; Maté-González, González-Aguilera, Linares-Matás, & Yravedra, 2019; Orlikoff, Keevil, & Pante, 2017; Otárola-Castillo et al., 2018; Pante et al., 2017; Yravedra, Aramendi, Maté-González, Austin Courtenay, & González-Aguilera, 2018; Yravedra et al., 2017). These are but a few examples of the ways in which anthropologists are using 3D models in their research.

3D scanning has had major impacts for cultural heritage and data sharing. Digital models can be shared electronically making them more accessible to researchers across the globe (Abel et al., 2011; Wrobel, Biggs, & Hair, 2019) through platforms such as MorphoSource, Virtual Anthropology, Sketchfab, Archaeology Data Service, Smithsonian3D, AfricanFossils.org, and tDAR. (For further discussion on 3D data repositories, see Bastir et al., 2019; Hassett, 2018; Wrobel et al., 2019). The ability to share digital models is especially pertinent for the maintenance of research continuity during events that limit travel such as the ongoing pandemic. Additionally, digital collections reduce the need for travel and thus the environmental impact of research. The ease with which models can be shared expands the possibilities for cultural heritage, education, science communication, and public engagement. Research quality 3D models can be

used to facilitate preservation by limiting the handling of the actual object (Means, McCuiston, & Bowles, 2013; Pletinckx, 2011). Furthermore, data collection from 3D models is inherently non-destructive (Wu & Schepartz, 2009). Not only are many repositories open-access resources, public institutions are increasingly creating virtual experiences that allow patrons anywhere in the world to explore archaeological sites and museums (e.g., the Bureau of Ocean Energy Management Virtual Archaeology Museum, the Turkish General Directorate of Cultural Assets and Museums, and the Black Heritage Trail. (A comprehensive list of virtual tours can be found on the Archaeological Institute of America's [online education resource list](#)). As a result of the push to create public-facing resources, publications have emerged describing methods for creating virtual exhibits and to explore ways in which 3D scanning can be used to engage the public (e.g. Abel et al., 2011; Bruno et al., 2010; Means et al., 2013; Quattrini et al., 2020; Tucci, Cini, & Nobile, 2011; Ynnerman et al., 2016; Younan & Treadaway, 2015). Additionally, options are becoming available for educators to develop content that is more accessible through the application of 3D printing (Bastir et al., 2019; Evelyn-Wright, Dickinson, & Zakrzewski, 2020; Weber, 2014). As the field grows, journals (e.g. *Digital Applications in Archaeology and Cultural Heritage*, the *Virtual Archaeology Review*, and *The Journal of Computer Application in Archaeology*), conferences and professional organizations (e.g. *Computer Applications and Quantitative Methods in Archaeology*) are being established that are specifically devoted to the advancement of digital methods in archaeology. Finally, the rapid growth of the field has inspired conversations on the ethics of and best practices for engaging in digital anthropology (See Dennis, 2020; Douglass et al., 2017; Hirst et al., 2018; Lewis, 2019; Quattrini et al., 2020; Richards-Rissetto & von Schwerin, 2017; Weber, 2014; White et al., 2018; Wrobel et al., 2019).

Photogrammetry, laser scanning, and structured light scanning are commonly used methods for creating 3D models of objects and are useful for creating high-resolution, textured scans. (See Evin et al., 2016; Jurda & Urbanová, 2016; Lauria, Sineo, & Ficarra, 2022; Linder, 2016; Magnani, Douglass, Schroder, Reeves, & Braun, 2020; McPherron, Gernat, & Hublin, 2009; Niven, Steele, Finke, Gernat, & Hublin, 2009; Porter, Roussel, & Soressi, 2016, 2019, for literature detailing these approaches to scanning.) However, objects are generally scanned individually and the scanning and post-processing times can be extensive. Bretzke and Conard (2012) demonstrated that two objects can be scanned at a time. In some cases, multiple objects can be scanned simultaneously using medical or micro-CT. The output Digital Imaging and Communications in Medicine (DICOM) files are then interactively surfaced and then separated into individual files and cleaned using expensive, proprietary and GUI-based software such as Slicer, Aviso, or Geomagic (Göldner, Karakostis, & Falcucci, 2022). In these cases the scanning process is efficient but at the cost of an increase in post-processing time and, like the other methods, is not conducive for efficiently creating a full set of 3D models of objects from large collections.

The ability to feasibly scan large collections like faunal assemblages, which can be comprised of over ten thousand specimens, necessitates a significant decrease in the time required for processing and post-processing. As such, scanning has been mostly restricted to small collections or a small subset of a large collection, which imposes limitations on research requiring larger sample sets. The ability to expediently scan and model specimens from large collections opens possibilities for new types of data accumulation, which in turn provides access to methods such as machine learning and other powerful computational approaches designed to handle larger and richer data sets (Carleo et al., 2019; Jordan & Mitchell, 2015; C. P. E. Zollikofer et al., 1998).

In this paper, we describe a method that we have developed, which we call the *Batch Artifact Scanning Protocol*, to safely and rapidly scan large assemblages of objects using a medical CT scanner. For our research purposes we scanned experimentally broken ungulate limb bones. The DICOM data are automatically segmented and surfaced using an algorithm that can be executed in MatLab or Python. Here we provide a step-by-step description of how to use the Batch Artifact Scanning Protocol, emphasizing key points necessary for achieving optimal results. We then discuss the factors to consider when weighing op-

tions for constructing 3D models for research and highlight when this approach is most useful. The purpose of this paper is to provide sufficient details in order to offer an inroad for those who are new to CT scanning, so that the Batch Artifact Scanning Protocol can be adopted and built upon by independent research groups.

## 2 Materials and Method

Here we describe in detail the steps and procedures in the Batch Artifact Scanning Protocol, as applied to scan and produce high resolution 3D surface models of 2,474 bone fragments drawn from a collection of experimentally broken ungulate appendicular long bones being used in research on how early hominins used bone marrow as a food resource.

This paragraph provides an outline of the steps taken throughout the process. Prior to scanning we assembled the required materials; chose the specimens we wished to scan; and, then bone fragments were placed in scan packets that were then transported to the scanning facility. They were scanned using medical Computed Tomography (CT). Subsequent DICOM data were processed using a Python algorithm that separated each fragment into individual files; segmented the fragment from the remainder of the image (what can be thought of as negative space); and, then the segmented images were surfaced to create a 3D mesh. Surfacing is the process by which scan data are converted into a solid object or mesh. These meshes were then checked and adjustments were made on individual fragments as needed. The time required for such manual interventions was minimized through our overall design of the scanning and segmentation protocols.

### 2.1 Prior to Scanning

#### 2.1.1 Assembling Required Materials

The following materials were needed to create the scan packets: large rolls of polyethylene foam, a glue gun, glue sticks, box cutters, and tape (we used painter's tape). Packets were labeled using a sharpie. The work was done on a large cutting mat to protect the surface of the work table. Large military grade duffel bags were used to transport scan packets to the facility where they were scanned. We also used a computer and camera (or smartphone) to document the fragment layout in a `.csv` file and take photos as backup (See [Figure 1](#)).

#### 2.1.2 Selecting Specimens to Scan

When choosing specimens for scanning, one of the most important factors to consider is scan resolution. The appropriate scan resolution is going to depend on the research question, the size of the object that needs to be scanned, the capabilities of the scanner, and the field of view used during scanning. Though it may seem counter-intuitive, the highest possible resolution is not always the best option. Optimal resolution depends on the scale required to address the question. Though high resolution scans can serve as a reference, and can always be decimated (i.e. the number of polygons in the mesh can be reduced) as required in order to streamline computational algorithms, they can radically increase computer processing times at all stages of the project, including the initial scanning, which may be prohibitive when working with large samples.

Running test scans is recommended to verify the minimum size required for achieving usable models. For our research purposes, we needed to capture the macromorphology of the bone fragment in order to extract global features and measure angles along the fractured edges of the fragment. We chose to scan fragments that are  $\geq 2$  cm in maximum dimension but we found that fragments  $\geq 5$  cm offered visually better models. Other considerations included how thin the bone is (i.e. areas of translucence) and the relative dimensions of the fragment. [Figure 2](#) illustrates the standard directional axes conventionally used in



Figure 1: Supplies needed for scanning

medical CT scanning to orient the subject of scanning on the bed. The  $x$  axis extends across the width of the bed. The  $y$  axis extends from ceiling to floor, and the  $z$  axis runs along the length of the bed. The bed moves along the  $z$  axis. An object that is oriented such that its longest dimension aligns along the  $z$ -axis will result in a better scan than an object with its shortest dimension aligned along the  $z$ -axis. This is an important consideration for scanning objects such as long bone fragments that tend to be longer than they are wide.

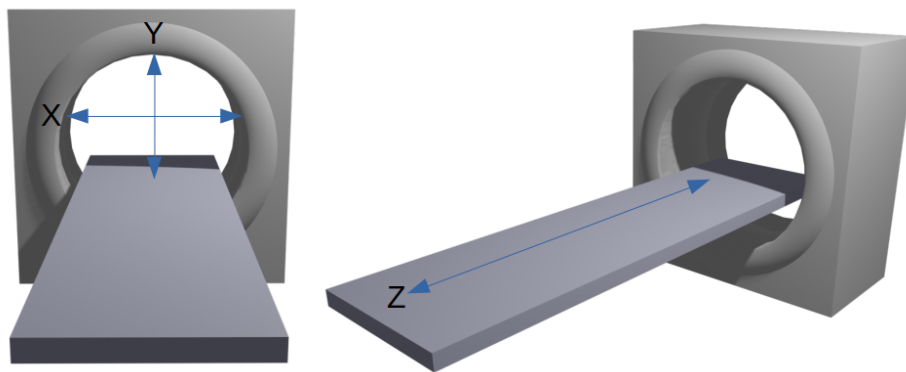


Figure 2: Directional axes used in CT scanning

Field of view is another important consideration (Miyata et al., 2020). As the package size in which the fragments are placed increases, the field of view required by the scanner increases along with it. If the increase in package size is due to an increase of the number of fragments in the packet, then the disparity in the size of each individual fragment and the field of view increases and causes the quality of the scan to decrease. This is less of an issue if the increase in the field of view is related to an increase in fragment size.

For this reason, we chose to create scan packets with similarly sized fragments and because the fragments were generally small we chose to limit the number of fragments in each packet.

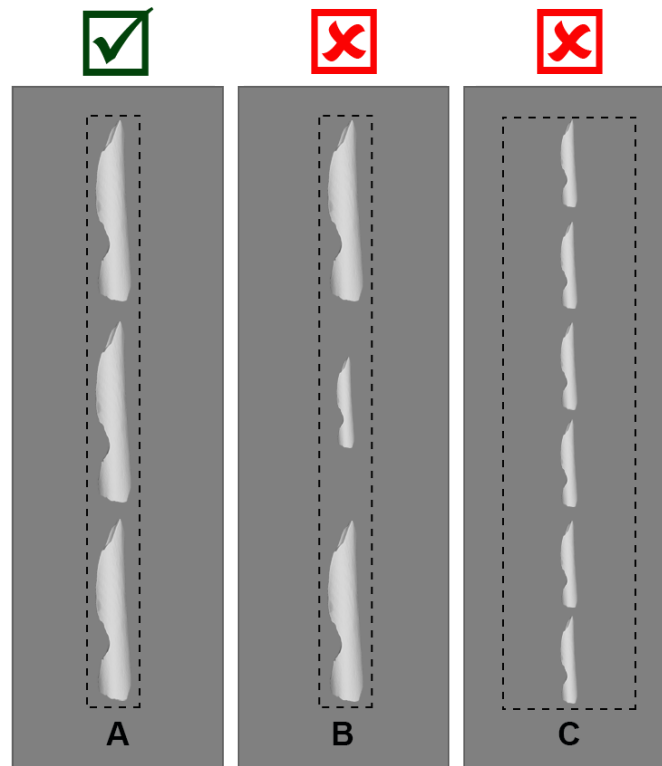


Figure 3: Field of view

For the best resolution, the boundaries of the field of view should be as close to the target objects as possible (A). If specimens are disparate in size, the resolution of the smaller specimens will diminish (B). If the field of view is wide, this will also compromise resolution (C).

### 2.1.3 Arranging Specimens for Packaging

Once the fragments were chosen, we packaged them in polyethylene foam for transport and scanning. We cut out strips of polyethylene packaging foam and laid the bone fragments linearly, end-to-end along the center of one of the foam strips. In order for the automated segmenting and surfacing algorithm to work properly, we allowed approximately 1-2 cm clearance between bone fragments in each packet. In order for the algorithm to successfully divide the scan into individual fragment files, there can be no overlap between specimens in the  $x$ - or  $y$ -directions (see Figure 4). The surfacing algorithm detects breaks between the fragments in the scan data and automatically separates the images according to those breaks. If there is overlap between two fragments the algorithm may not recognize them as two fragments and may combine them into a single fragment or cut off parts of one or both fragments. We also ensured a 3 – 5 cm margin along the edges of the packaging material to accommodate the glue used to seal the packets closed.

For each packet, we chose fragments that are similar in size in the  $x$ - and  $y$ -direction in order to conserve material because several strips of foam were used for each packet. We stacked the foam strips one on top

of the other until the stack was high enough to comfortably cover the utmost top edge of the fragment thus providing protection for the specimen in all directions.



Figure 4: Fragment placement

The fragments should not overlap the clearance zone.

#### 2.1.4 Documenting Specimens Prior to Packaging

Once the bone fragments were arranged in the desired order along the first packaging strip, the specimen catalog number was recorded in a `.csv` file (see [Figure 5](#)). (A template can be downloaded from the [AMAAZE website](#) and [GitHub](#).) It is essential to adhere to the prescribed `.csv` file format in for the algorithm to function properly. It is equally important to label the "head" of the packet such that it is placed properly on the CT scanning bed. Each line item in the `.csv` file is dedicated to one packet and the algorithm reads the line from left to right (preferably "head" to "foot" on the scanning bed). Therefore the leftmost entry in the `.csv` file is generally at the "head" of the packet. Should there be an error when the packet is placed on the bed such that it is scanned from "foot" to "head", then the entry for the column labeled "CTHead2Tail" should be changed to R2L so that the line is read in the opposite direction.

We took photographs of how the fragments were laid out on the foam strip for reference and back-up in case there were errors when recording information in the `.csv` file. A wide angled shot of the entire layout of the package was taken, with the package number displayed in the front and center of the image (see [Figure 6A](#)). Pictures of the layout of each fragment were taken as well. The specimen number for the individual bone fragment was clearly visible in the image, along with a part of the previous bone specimen for context (see [Figure 6B](#)). For fragments that were not directly labeled, the bag with the specimen number of the bone was placed above the fragment in the picture (see [Figure 6C](#)).

#### 2.1.5 Packaging Specimens for Transport and Scanning

Once the layout was established and recorded, we carefully used a sharpie to trace the fragments, being mindful not to get ink on the fragments (see [Figure 6E](#)). The outlines can be slightly larger than the fragment itself. For smaller fragments, a thin tip sharpie can be used in order to produce a more accurate outline. After outlining, the specimens were removed from the strip and set aside. All but two of the remaining foam strips were glued to the back of the outlined strip using a glue gun. This ensures that the strips will form one cohesive stack. Once the glue set, we followed the outlines using box cutters to cut holes in the stack of glued foam. The foam that was removed was set aside in the order that it was cut out so that it could be used later in the process to add padding if needed (see [Figure 6F](#)).

1	CT	ScanPacket	CTHead2Tail	Mirrored	1	2	3	4
2	CT20180813	8	L2R	no	MN18040205	MN18040206	MN18040207	
3	CT20180813	10	L2R	no	MN10AA2404	MN10AA2504	MN10AA2507	MN10AA2

Figure 5: Documenting specimens for scanning

An example of how to complete the formatted `.csv` so that the segmentation and surface algorithms will function properly.

After the foam had been cut to create cavities for each bone fragment, the styrofoam stack was flipped upside down to properly attach the bottom piece of the structure. One of the single strips of styrofoam previously set aside was used for the bottom piece. When specimens were heavier, we added additional layers to the bottom and top to prevent the bone fragments from falling out of the packaging during transport and scanning. In some cases, especially when packaging smaller fragments, we cut out the cavities prior to gluing so that we could apply glue near to the edges that were cut to ensure that fragments would not escape the cavity and slip in between the layers of foam.

Having securely glued the base to the bottom of the package, the stack was flipped right side up and the first specimen cavity (i.e. the "head") was placed to the left side to remain consistent with the format in the `.csv` file. We placed individual bone fragments into their corresponding cavities in the same orientation in which they were outlined. Care was taken to place the specimens so they were not likely to move around in transit. As needed, the excess pieces of foam taken from the outline cuttings were used to fill in any gaps between the edge of the cavity and each fragment. This was to prevent unintentional damage related to movement in the cavity and to ensure alignment of the fragments along the z-axis.

Once satisfied with the placement of the bones inside the package and their relative inability to move around in transit, the final foam strip was secured to the top of the package. Care was taken not to get glue on the fragments. After constructing the packet, we wrapped a strip of painter's tape around the entire shorter circumference at the head of the packet then labeled the tape with the packet number (see [Figure 7](#)) and the word "head" so that the CT technicians we worked with knew how to place the packet on the scanning bed and what number to use in the filenames for the output data. Additional strips were added to any section of the packet for added protection especially in areas that seemed unstable or likely to come apart, such as in between two larger bones or in the middle of long bones that were at risk of breaking (see [Figure 6D](#)). The completed packets were ready to go to the scanning facility (see [Figure 8](#)).

## 2.2 Scanning

We brought a total of 2,474 bones fragments in 331 packets to the Center for Magnetic Resonance Research at the University of Minnesota. Each packet was scanned individually. Each scan takes a couple minutes including the time it takes to lay the packet on the scan bed, adjust the field of view, and take the scan. Once all scans were completed the data were exported as DICOM files.



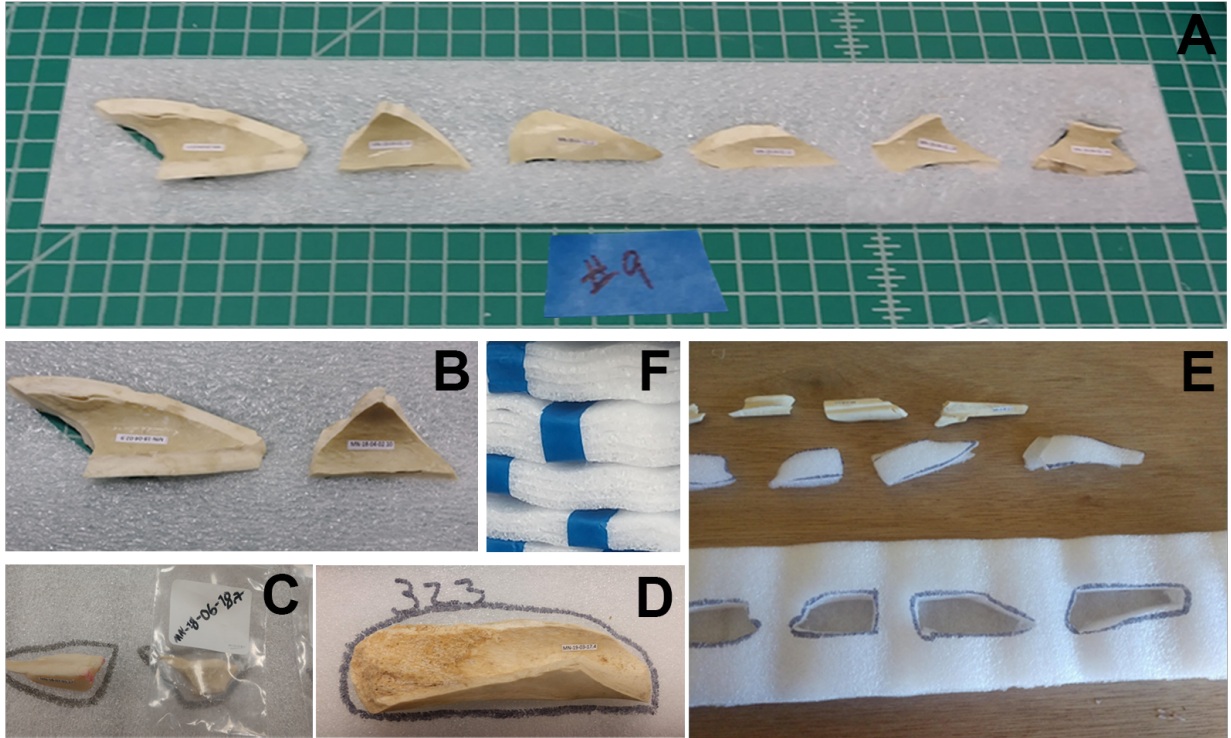


Figure 6: Fragment layout

We took a photograph of the layout of the fragments for the entire package (A). Photographs were taken of individual fragments such that we could clearly see the labels (B). If the fragment was not directly labeled we included the labeled bag in the photograph (C). We traced the fragments using a sharpie (D) and then used the outline to cut out sections in the foam to encase the fragments (E).

Packets were wrapped in tape for additional protection (F).

Table 1: CT Parameter Settings

PARAMETER	SETTING
SLICE THICKNESS	0.6
RECONSTRUCTION INTERVAL	0.6 MM
KV	80
MA	28
ROTATION TIME	0.05 SEC
PITCH	0.8
ALGORITHM	BONE WINDOW
CONVOLUTION KERNEL	B60F-SHARP

A Siemens Biograph 64 slice PET/CT was used to scan the packets. The scanning parameters are provided in Table 1. Here we offer simple descriptions of these parameters to provide a basic understanding of how they affect image capture. However, using medical CT scanning will require working with a trained radiologist who can determine the appropriate settings for achieving an optimal image. A basic understand-



Figure 7: Example of package label



Figure 8: Packets ready to go to scanning facility

ing of these parameters can be useful for discussing the needs that are particular to the project with the radiologist, e.g. capturing trabecular bone, working with fossilized material, and navigating matrix in-fill or adhesion, all of which can be effectively mitigated using CT. For more detailed, technical descriptions of how CT scanning works, see [Buzug \(2011\)](#); [Scherf \(2013\)](#); [Sera \(2021\)](#); [Spoor, Jeffery, and Zonneveld \(2000\)](#); [Withers et al. \(2021\)](#).

The CT machine captures images by sending a narrow X-ray beam through the target object, in this case bone fragments. It differs from a standard X-ray in that the beam rotates around the target object as the scanning bed moves along the  $z$  axis, creating cross-sectional images with every rotation, referred to as slices. Slices can be stacked to create a 3D image.

Rotation time refers to the time it takes for the beam to rotate around the target object. Slice thickness, as the name suggests, refers to the thickness of a single slice or cross-sectional image. The reconstruction interval, or slice increment, is the distance that the bed moves with each slice. If these values are equal, the slices are contiguous. If the reconstruction interval is smaller than the slice thickness, then there will be overlap between slices. If the interval is larger than the slice thickness, then there will be a gap between the

slices and the information in between must be interpolated from the captured data. Smaller slice thicknesses improve the quality of the image but run the risk of increasing noise (Alshipli & Kabir, 2017; Lalondrelle et al., 2012).

Pitch refers to the relationship between the rotation speed and the table movement. Using helical scanning causes what is called "slice broadening" because of the spiraling path (as opposed to a closed ring) used in each slice. In the case of the helical scan, the reconstruction interval is determined by the data obtained during scanning since the z-position changes within a single rotation of the scan and the z-position that starts a slice is based on the projection used to start the slice (see Figure 9). If the value of the pitch is less than 1, then slices overlap. If it is equal to 1 then they are adjacent. If it is greater than 1, then there are gaps between the slices. Decreasing pitch improves resolution but increases radiation exposure. Given that radiation exposure was not a concern for the bone fragments we chose a minimal value (0.8).

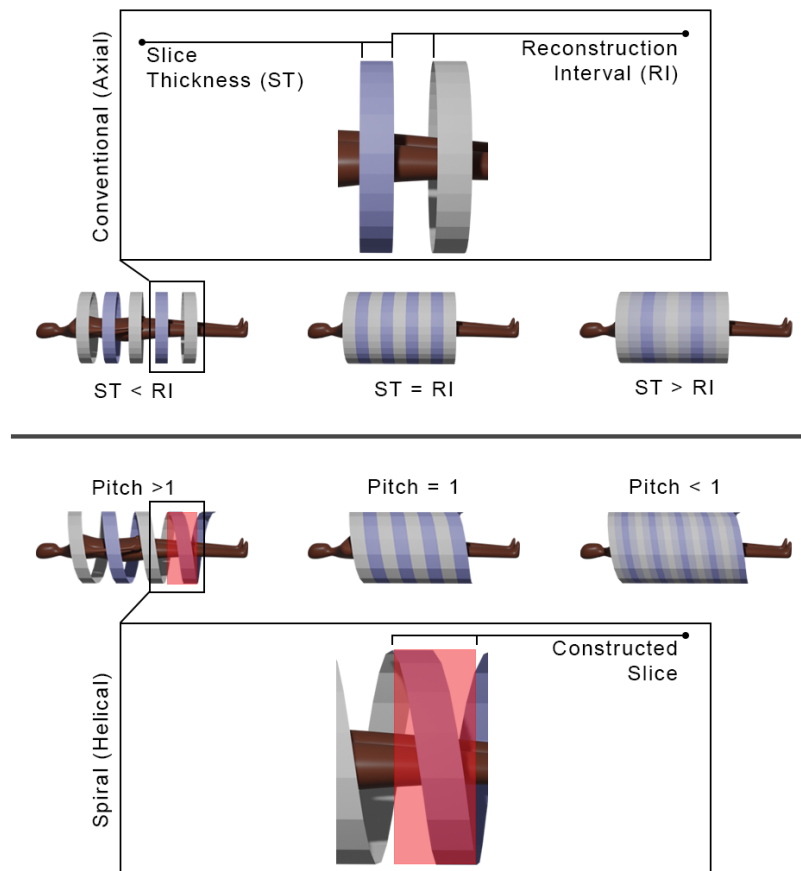


Figure 9: CT scanning

The top portion of this figure illustrates Conventional CT scanning whereas the bottom portion illustrated Spiral CT scanning. In either case, if the pitch is greater than 1 or the slice thickness is less than the reconstruction interval, there will be space between the slices. If the pitch is equal to 1 or the slice thickness and reconstruction interval are equal then the slices will be contiguous. If the pitch is less than 1 or the slice thickness is greater than the reconstruction interval, then the slices will overlap.

Kilovoltage (KV) refers to the tube voltage, or the strength, of the x-ray beam and milliampere-seconds (MA) refers to the rate of radiation produced per second. These values are complementary values that can be adjusted to control the trade-off between the quality of the image and radiation dosage. The kilovoltage, which generally ranges between 50 - 120, must be high enough for sufficient penetration and contrast between tissues, but not so high that it subjects the patient to an unnecessary level of radiation. Denser materials require higher KV values. The KV value can be adjusted to achieve the appropriate amount of contrast, which can be thought of in terms of the gradients between white and black. High contrast produces stark white and black images without shades of gray in between, while a low contrast image is going to look muddled and gray. Higher rates of radiation exposure related to KV can be offset by lowering the MA which measures how much radiation is produced per second and effects radiographic density (or blackening of the image). Increasing the MA makes the film darker. For example, a radiograph of an intact long bone, the compact bone should appear whiter than the internal marrow (medullary) cavity and the intermediate spongy bone. In an underexposed radiograph with MA values that are too low, the bone will appear whiter throughout, making it difficult to distinguish these structures and in bones that are overexposed with an MA value that is too high, these structures might be altogether undetected or if they are detected appear to be thinner or less extensive structures. In both the under- and over-exposed cases, differentiating the boundaries between the medullary cavity and the compact bone is difficult. Additionally, in the case of overexposure, differentiating the bone from the surrounding space is a challenge. The radiologist is trained to make such adjustments so as to achieve optimal results. To help them in this regard, it is useful to have a discussion about what types of data will be extracted from the images and which skeletal features are most important. This can be especially important when working with matrix infill, adhering matrix, and fossilized material since these are not typically found in medical contexts.

The convolution kernel is an algorithm that is used to sharpen an image and different kernels have been developed for different types of tissues. A higher value will offer a sharper image but can increase noise. Again, the radiologist can choose the best option based on the object to be scanned.

### **2.2.1 Additional Considerations when CT scanning**

The Hounsfield Unit is a key concept of CT scanning that refers to radiographic density ([Scherf, 2013](#)). Materials are associated with specific Hounsfield units. Water sets the starting point at 0 HU. Materials with lower radiodensity such as Fat have a negative Hounsfield unit (-120 to -90). Cancellous bone ranges from 300 to 400 HU and cortical bone ranges from 500 to 1,900 HU, therefore it is necessary to consider variation in the composition of the object to be scanned. This is especially important when CT imaging osteological materials and fossils coming from archaeological contexts. Bones that have fossilized may require different HU values than fresh bone ([Spoor et al., 2000](#)). Additionally, if adhering matrix has a similar Hounsfield unit as the fossil, then they will be difficult to distinguish using CT. Conversely, in situations where the HU values are different, CT can be a way to "remove" adhering matrix without damaging the fossil ([Conroy & Vannier, 1984](#); [C. P. E. Zollikofer et al., 1998](#)). In fact, this is something to bear in mind when choosing the materials for creating scan packets. Whether it be adhering matrix or packaging material it is necessary for the HU to differ from that of the target object.

An important parameter for the CT scanner is the field of view. By narrowing the field of view so that the scan is tightly focused around the line of bone fragments on the scanning bed, we can obtain higher resolution images compared to using a field of view that encompasses the whole width of the bed. We have experimented with placing multiple packets on the scanning bed beside each other, in order to scan more objects in parallel, but the larger field of view required for such a setup resulted in extremely low resolution CT images that were not sufficient for surfacing a majority of the bone fragments of interest. In practice, this means that smaller fragments require smaller packets as opposed to using equivalently sized packets and adding more fragments. Our CT scans have a resolution of 0.6mm between slices (along the direction

of the scanning bed), and approximately 0.15mm resolution within slices with a narrow field of view. It is possible that with a much higher resolution CT scanner, multiple packets could be scanned in parallel while maintaining sufficient resolution.

## 2.3 Post Processing

Detailed written instructions for creating the 3D models from the DICOM scan data can be found on the [AMAAZE GitHub](#) along with the AMAAZEtools package required to run the CT-Surfacing scripts in Python. Installation instructions accompany the packages on the AMAAZE GitHub. We have also provided data from two scans (scans 8 and 10), each containing four fragments, and an accompanying `.csv` file so users can try the process without having their own DICOM data. In summary, to begin the process of surfacing the scans to create the models, the AMAAZEtools packages must be installed and one must have the appropriate DICOM files and the properly formatted `.csv` file.

The first step is to separate the multi-fragment files into single-fragment files. This is done by running the Python script called `dicom_firstpass.py`, which automatically segments the file into individual fragments and outputs images of the segmentation with bounding boxes (see [Figure 10](#)), as well as the bounding box coordinates, as a `.csv` file which can be manually edited as needed.

The algorithm for automatically separating multiple bone fragments from a single CT scan works by first thresholding the CT image at a user-specified value in Hounsfield units (HU). The specific threshold depends on the material under consideration; for bone fragments we use 2000 HU. The thresholded binary images are then projected onto each 2-dimensional view of the length of the scanning bed, and the bone bounding boxes are identified by taking the largest connected components of the projected binary images and adding padding on each side. See [Figure 10](#) for a depiction of the computed bounding boxes for each bone for the test scan provided in GitHub.

The automatic algorithm works very well, but there can be occasions when the automatically detected bounding boxes are incorrect. In this case, adjustments can be made by editing the `ChopLocations.csv` file that was automatically generated by `dicom_firstpass.py` prior to the next step in the processing. After modifying the `ChopLocations.csv`, the script `dicom_refine.py` will generate new bounding boxes based on the modified data in the chop locations file. This process can be iterated several times, if necessary, until the bounding boxes are correct. Again, let us emphasize that the failure cases in the method are very rare and a vast majority of the time, no refinements are needed.

Once the files are segmented properly, the next step is to run `surface.py` to generate triangulated surface 3D models for each object in the CT scan. The surfaces are generated from the CT images with the Marching Cubes algorithm [Lorensen and Cline \(1987\)](#). The user must provide a threshold parameter (called `iso` in the code) for the surfacing. As in the segmentation part above, the `iso` threshold value is material dependent, and may also depend on the size of the objects, amount of fine detail, and the resolution of the CT scanner. For surfacing bone fragments we normally use `iso=2500`, with some manual adjustments in special cases. The surfacing script reads the CT resolutions, which are often different between slices, compared to within each 2D slice, from the DICOM header files and scales the resulting mesh so that the units are millimeters in all coordinate directions.

Choosing good thresholds is largely application dependent. Larger threshold values may omit fine scale details, while small threshold values will pick up on noise and scanning artifacts. When scanning bone fragments, lower values are useful when the bone is extremely thin or more porous and lower values capture trabecular bone better than higher values.

The `surface.py` script also has the capability to generate rotating animations (as `gif` files) of each object that has been surfaced. All the meshes are output as individual `.ply` files.

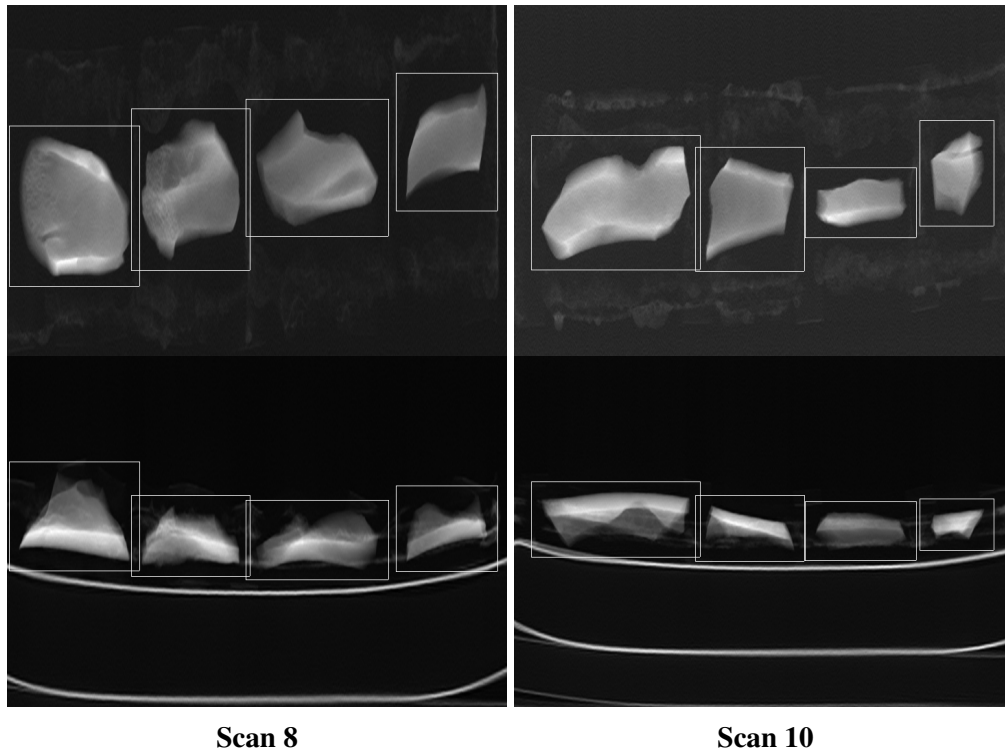


Figure 10: Automated segmentation

Examples of the .jpg images output by the automated segmentation algorithm. These examples come from a session during which we scanned multiple packets. These scans come from packets 8 and 10 in that series.

### 3 Discussion

Choosing an appropriate scanning method for research requires, at minimum, a consideration of the following: (1) portability if required; (2) cost; (3) time; (4) computational resources, including memory, speed, GPU, and storage; (5) whether or not texture is needed; (6) required scan resolution; and (7) the geometry that needs to be captured.

The location of the collection that needs to be scanned is the first concern. If the collection cannot be transported to a scanning facility then the scanning equipment must be transported to the collection which eliminates the opportunity for CT scanning. In these cases, the time to scan can increase considerably especially when working with large collections.

Primary considerations when engaging in 3D scanning are how much time and how much money it will take. Methods like photogrammetry are extremely cost effective (Porter et al., 2016). Photogrammetry, laser scanners and structured light scanners are portable and can be taken into the field. However, they are limited to scanning a single object at a time; moreover, it takes a considerable amount of time per scan as compared to the method presented here. Although this is not so problematic when the sample size is small, zooarchaeological assemblages can contain  $> 10,000$  specimens, thus making the use of portable scanners untenable. The method presented here thus fills a niche where large quantities of research-quality models need to be created from specimens that can be transported to a CT scanning facility.

Very few medical CT and microCT scanners are portable and it was too cost prohibitive to purchase the equipment ( $\geq 100,000$  USD) ourselves. Therefore, to use the Batch Artifact Scanning Protocol, we made

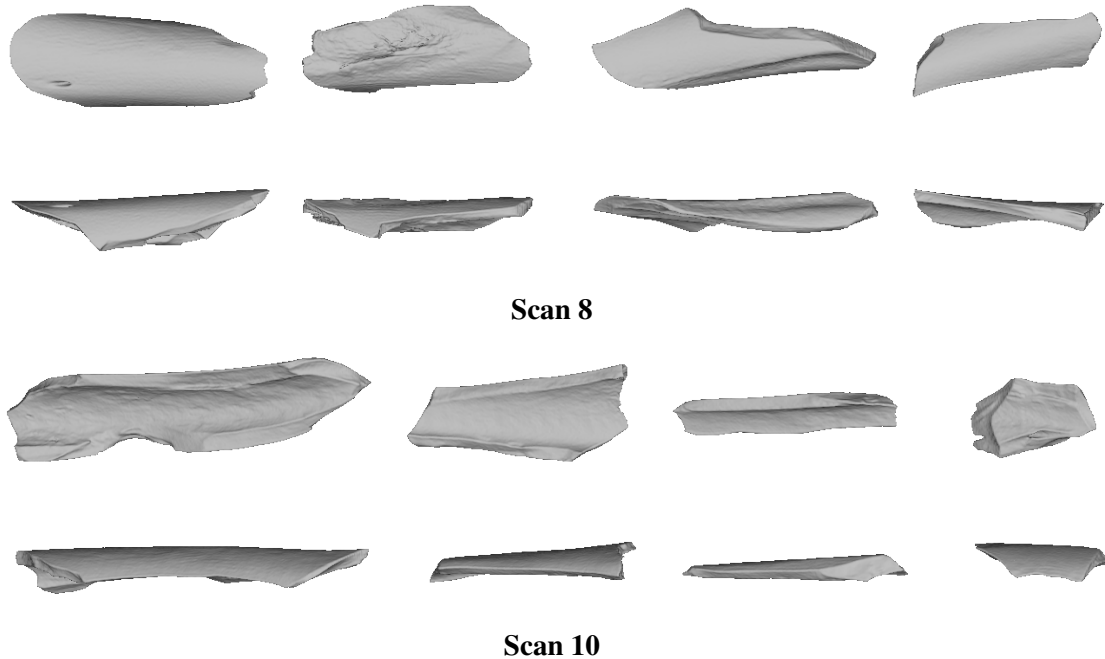


Figure 11: The final meshes for scans 8 and 10

arrangements to transport specimens to medical scanning facilities and paid fees for scanning services. In total, 331 packets were required to transport and scan 2,474 bone fragments. Some facilities will charge per scan and others will charge an hourly rate and rates can vary considerably among institutions and departments. By choosing an hourly rate we were able to scan 2,474 specimens in 93.75 hours for 2900 USD.

Several attempts at photogrammetry proved to be ineffective due to issues of translucency and reflectivity so those calculations are not provided here. [Porter et al. \(2016\)](#) used photogrammetry to scan lithic tools and reported a total scanning time of 12 minutes with variable post-processing times. [Kingsland \(2020\)](#) compared three software used in photogrammetry (Agisoft Metashape, Bentley ContextCapture, and RealityCapture) and reported average post-processing times ranging from 63 – 133 minutes per object.

We scanned fragments using the David structured light scanner and David software on a highend desktop (Dell computer with Microsoft Windows 10 Enterprise OS, 2.7 Quad-Core Intel Core i7, 128 GB RAM). Images were captured every 15° with a total of 24 captures per 360° rotation. We found that it takes approximately 5 – 10 minutes to set up the specimen. Scanning takes between 15 – 25 minutes. Typically, it takes at least two rounds of scanning to capture the entire fragment because the fragment needs to be flipped after the first round to capture the portion that was mounted and inaccessible to the scanner in the first round. Once scanning is complete, post-processing is required. For this we used the David software in conjunction with Geomagic Design X, a CAD software. The time it takes to post process can vary considerably based on the degree to which the scans need to be cleaned and the number of challenges that arise during alignment and registration (see [Bernardini & Rushmeier, 2002](#)). Based on our experience, it takes on average between 15 – 60 minutes to post-process the scans to create the 3D model. To set-up, scan and post-process 2,474 fragments to make 3D models would minimally take 2,061.5 hours of interactive user time, or 50 minutes per fragment. These times are similar to times reported elsewhere (see [Ahmed, Carter, & Ferris, 2014](#); [Bretzke & Conard, 2012](#); [Kuzminsky & Gardiner, 2012](#); [Magnani, 2014](#)).

On the other hand, with the CT scanning method described here, each packet takes between 15 – 30 minutes to assemble. We ended up with a total of 331 packets, which is about 7 fragments per packet; it

Table 2: Comparison of Scanning and Processing Times

	BATCH ARTIFACT SCANNING PROTOCOL <sup>1</sup>	STRUCTURED LIGHT/ LASER SCANNER <sup>2</sup>
TOTAL NUMBER OF SPECIMENS	2,474	2,474
SPECIMEN SET UP	83 HOURS	206 HOURS
SCANNING TIME	10.75 HOURS	1,237 HOURS
POST-PROCESSING TIME	< 3 HOURS	618.5 HOURS
TOTAL TIME	96.75 HOURS	2,061.5 HOURS
TIME PER FRAGMENT	0.04 HOURS (2.35 MIN)	0.83 HOURS (50 MIN)

<sup>1</sup>Calculated from actual time it took to scan 2,474 fragments.

<sup>2</sup>Calculated based on times taken to scan fragments using the David Structured White Light Scanner. Times multiplied to predict total time it would take to scan 2,474 fragments. This would be a calculation of the minimum time it would take.

took a total of 83 hours to assemble them, and 10.75 hours to scan. The post processing is very fast; it takes 35 seconds to surface all 8 bone fragments in the example GitHub repository using a standard laptop computer, amounting to about 4.375 seconds per fragment. To surface the whole collection consisting of 331 packets and 7 fragments per packet takes slightly under 3 hours. This means that to create a single 3D model of a bone fragment using laser and structured light scanners takes 50 minutes and less than 3 minutes using medical CT (see [Table 2](#)).

Computational expenses are another important consideration and are largely centered on memory and processing power (e.g. memory, storage, GPU, and speed). We have found that DICOM files require approximately 100MB of storage space per bone fragment, but of course this depends on resolution. Thus, the collection described in this paper takes roughly 250GB of storage space for the DICOM files on disk. After surfacing to create 3D triangulated surfaces for each object, the resulting meshes take on average 10MB per fragment. For our purposes, we purchased two 2 TB external drives to transport files from the scanning facility so that we could surface them on our computers. The Batch Artifact Scanning Protocol does not require any visualization software packages as part of the post processing, which generally require some form of GPU. For example, Geomagic requires a GPU with a minimum of 2GB of memory, and in some cases 4GB, and Aviso requires a GPU with a minimum of 1GB. Running the surfacing step of the Batch Artifact Scanning Protocol involves purely CPU computations, and hence the post-processing can be performed on any computer without a GPU. On a high end laptop computer (MacBook Pro, 2 GHz Quad-Core Intel Core i5, 32 GB RAM) we were able to process each bone fragment in 4.375 seconds. Of course, faster computers and parallel processing can be used to accelerate the process, as needed.

Beyond the logistics of scanning, it is necessary to consider what types of data need to be collected from the object. In particular, one must decide whether texture is required, determine the level of resolution required to answer the research question, and choose the parts of the object that need to be captured, in particular whether or no internal structures need to be captured. [Bernardini and Rushmeier \(2002\)](#).

In the simplest description, image texture refers to the perceived textures that are visible when looking at the object in real life (see [Figure 12](#)) and, in image processing, are defined by a series of texture units that describe a pixel (vertex or voxel) and its neighborhood [He and Wang \(1991\)](#). Because our research focuses on the analysis of shape, we had no need to capture texture making CT a viable option. The laser scanners and structured light scanners can oftentimes capture texture, however, this will increase processing times. The estimates provided in [Table 2](#) are based on fragments that were, in both cases, scanned without capturing texture.

Resolution can be thought of as the level of detail present in the model; higher resolution offers more



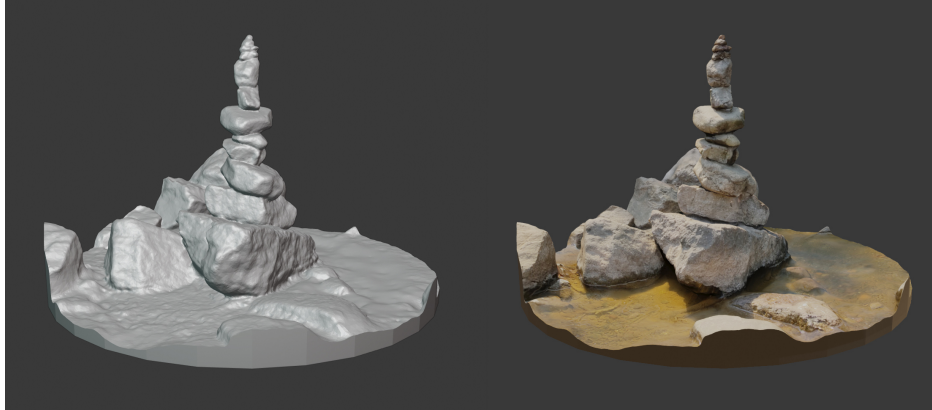


Figure 12: Texture

This is a 3D mesh of a rock cairn at Gooseberry Falls. The image on the left is without texture. The image on the right has texture. Scanning and 3D model created by Dr. Samantha Porter.

detail. A mesh is comprised of a certain number of points, oftentimes referred to as vertices, and the interpolated information in between those points. More points within a given area increase the detail of the model. That said, higher resolution is not always necessary and adds time to computational processes when working with the model. If one were to model a plane, only three points would be necessary to uniquely specify it. However, as the object increases in complexity, more points are needed to capture that complexity.

An equally important consideration pertaining to resolution is scale. One can imagine zooming in on an image of the eastern coastline of Florida. As one zooms in, the general outline between land and water will appear, then more curves along the shoreline will become visible, and ultimately one would be able to see the outline of individual grains of sand. If all that is needed is the general outline, then it would be computationally expensive to capture detail enough to see the grains of sand. Therefore, it is wise to consider the scale at which the research is being conducted and the required level of detail. That said, the Batch Artifact Scanning Protocol can be applied to images captured using micro-CT.

Consideration of the structural features that need to be captured may dictate which scanning method makes most sense. Structured light scanners and photogrammetry can only capture the outside surface of the objects, i.e. that which can be seen by the naked eye. On the other hand, CT captures the internal geometry making it useful for scanning internal anatomy or encased objects. Long bone shaft fragments can sometimes come in the form of cylinders which are more easily captured using CT. Researchers who wish to study internal structures such as endocrania require CT scans and approaches to 3D imaging described here (e.g. [Bräuer et al., 2004](#); [Conroy & Vannier, 1984](#); [Conroy, Vannier, & Tobias, 1990](#); [Conroy et al., 2000, 1998](#)).

### 3.1 Adapting this Approach

While we have thus demonstrated how the Batch CT Scanning Method can be applied to rapidly scan large collections of bone fragments using medical CT, scans from micro-CT can also be post-processed in the same manner. Furthermore, CT scanning is not restricted to bone. [Abel et al. \(2011\)](#) used micro-ct to create 3D models of lithic artifacts.

We described in detail how to effectively package specimens for safe transport and quick scanning,

however, this particular approach is not entirely necessary. What is required is that the specimens do not overlap between specimens in the  $x$ - or  $y$ -directions and that they are accurately recorded in the `.csv` file. Packaging specimens together may not make sense for much larger objects. Packaging is recommended to limit set-up time at the scanning facility which has the potential of increasing the financial expense, especially if the charge is per hour. And, it is recommended to keep the object safe during transport and handling at the imaging facility. When packaging is used the HU needs to be different from that of the objects that are being scanned.

## 4 Conclusion

Here we have presented the Batch Artifact Scanning Protocol, a new method for scanning and automatically surfacing large collections, using ungulate bone fragments as an example. This is especially important within zooarchaeology and taphonomy because collections are oftentimes large, exceeding 10,000 specimens. Additionally, the Batch Artifact Scanning Protocol can expedite the push toward data sharing and the building of large online databases making methods such as machine learning viable options for areas within anthropology that have previously suffered from insufficient sample sizes. The Batch Artifact Scanning Protocol also has implications for cultural heritage, education, and public-facing institutions such as museums. Collections can be scanned efficiently saving institutions time and money. Preservation of materials improves when researchers can use 3D models instead of handling the actual objects. 3D models can be used for educational purposes in formal and non-formal settings thus making connections with the broader public.

**Acknowledgments** We would like to thank all who helped bring this project to fruition. The bone fragments used in scanning were sourced from Scott Salonek with the Elk Marketing Council and Christine Kvapil with Crescent Quality Meats. Bones were broken by hyenas at the Milwaukee County Zoo and Irvine Park Zoo in Chippewa Falls, Wisconsin and various math and anthropology student volunteers who broke bones using stone tools. Sevin Antley, Alexa Krahn, Monica Msechu, Fiona Statz, Emily Sponsel, Kameron Kopps, and Kyra Johnson helped clean, curate and prepare fragments for scanning. Thank you to Cassandra Koldenhoven and Todd Kes in the Department of Radiology at the Center for Magnetic Resonance Research (CMRR) for CT scanning the fragments. Pedro Angulo-Umaña and Carter Chain worked on surfacing the CT scans. Matt Edling and the University of Minnesota's Evolutionary Anthropology Labs provided support in coordinating sessions for bone breakage and guidance for curation. Abby Brown and the Anatomy Laboratory in the University of Minnesota's College of Veterinary Medicine provided protocols and a facility to clean bones. Thank you to Samantha Porter who provided feedback on the manuscript.

**Funding Information** We would like to thank the National Science Foundation NSF Grant DMS-1816917 and the University of Minnesota's Department of Anthropology for funding this research.

## References

- Abel, R. L., Parfitt, S., Ashton, N., Lewis, S. G., Scott, B., & Stringer, C. (2011). Digital preservation and dissemination of ancient lithic technology with modern micro-CT. *Computers & Graphics*, 35(4), 878–884.
- Ahmed, N., Carter, M., & Ferris, N. (2014). Sustainable archaeology through progressive assembly 3D digitization. *World Archaeology*, 46(1), 137–154.
- Alshipli, M., & Kabir, N. A. (2017). Effect of slice thickness on image noise and diagnostic content of single-source-dual energy computed tomography. In *Journal of physics: Conference series* (Vol. 851, p. 012005). IOP Publishing, Bristol, UK.
- Amano, H., Kikuchi, T., Morita, Y., Kondo, O., Suzuki, H., Ponce de León, M. S., ... Ogihara, N. (2015). Virtual reconstruction of the Neanderthal Amud 1 cranium. *American Journal of Physical Anthropology*, 158(2), 185–197.
- Aramendi, J., Maté-González, M. A., Yravedra, J., Ortega, M. C., Arriaza, M. C., González-Aguilera, D., ... Domínguez-Rodrigo, M. (2017). Discerning carnivore agency through the three-dimensional study of tooth pits: Revisiting crocodile feeding behaviour at FLK-Zinj and FLK NN3 (Olduvai Gorge, Tanzania). *Palaeogeography, Palaeoclimatology, Palaeoecology*, 488, 93–102.
- Arriaza, M. C., Aramendi, J., Maté-González, M. Á., Yravedra, J., Baquedano, E., González-Aguilera, D., & Domínguez-Rodrigo, M. (2019). Geometric-morphometric analysis of tooth pits and the identification of felid and hyenid agency in bone modification. *Quaternary International*, 517, 79–87.
- Arriaza, M. C., Yravedra, J., Domínguez-Rodrigo, M., Maté-González, M. Á., Vargas, E. G., Palomeque-González, J. F., ... Baquedano, E. (2017). On applications of micro-photogrammetry and geometric morphometrics to studies of tooth mark morphology: The modern Olduvai Carnivore Site (Tanzania). *Palaeogeography, Palaeoclimatology, Palaeoecology*, 488, 103–112.
- Baab, K. L., McNulty, K. P., & Harvati, K. (2013). *Homo floresiensis* contextualized: A geometric morphometric comparative analysis of fossil and pathological human samples. *PLoS One*, 8(7), e69119.
- Baab, K. L., McNulty, K. P., & Rohlf, F. J. (2012). The shape of human evolution: A geometric morphometrics perspective. *Evolutionary Anthropology: Issues, News, and Reviews*, 21(4), 151–165.
- Barone, S., Neri, P., Paoli, A., & Razonale, A. V. (2018). Automatic technical documentation of lithic artefacts by digital techniques. *Digital Applications in Archaeology and Cultural Heritage*, 11, e00087.
- Bastir, M., García-Martínez, D., Torres-Tamayo, N., Palancar, C., Fernández-Pérez, F. J., Riesco-López, A., ... López-Gallo, P. (2019). Workflows in a virtual morphology lab: 3D scanning, measuring, and printing. *Journal of Anthropological Sciences*.
- Bello, S. M. (2011). New results from the examination of cut-marks using three-dimensional imaging. In *Developments in Quaternary Sciences* (Vol. 14, pp. 249–262). Elsevier, Amsterdam.
- Bello, S. M., Parfitt, S. A., & Stringer, C. (2009). Quantitative micromorphological analyses of cut marks produced by ancient and modern handaxes. *Journal of Archaeological Science*, 36(9), 1869–1880.

- Bello, S. M., & Soligo, C. (2008). A new method for the quantitative analysis of cutmark micromorphology. *Journal of Archaeological Science*, 35(6), 1542–1552.
- Benazzi, S., Bookstein, F. L., Strait, D. S., & Weber, G. W. (2011). A new OH5 reconstruction with an assessment of its uncertainty. *Journal of Human Evolution*, 61(1), 75–88.
- Benazzi, S., Gruppioni, G., Strait, D. S., & Hublin, J.-J. (2014). Virtual reconstruction of KNM-ER 1813 *Homo habilis* cranium. *American Journal of Physical Anthropology*, 153(1), 154–160.
- Benazzi, S., Orlandi, M., & Gruppioni, G. (2009). Virtual reconstruction of a fragmentary clavicle. *American Journal of Physical Anthropology*, 138(4), 507–514.
- Berger, L. R., Hawks, J., de Ruiter, D. J., Churchill, S. E., Schmid, P., Deleuzene, L. K., . . . Zipfel, B. (2015). *Homo naledi*, a new species of the genus *Homo* from the Dinaledi Chamber, South Africa. *eLife*, 4, e09560.
- Bermúdez de Castro, J. M., Martín-Francés, L., Modesto-Mata, M., Martínez de Pinillos, M., Martín-Torres, M., García-Campos, C., & Carretero, J. M. (2016). Virtual reconstruction of the Early Pleistocene mandible ATD 6-96 from Gran Dolina-TD 6-2 (Sierra de Atapuerca, Spain). *American Journal of Physical Anthropology*, 159(4), 729–736.
- Bernardini, F., & Rushmeier, H. (2002). The 3D model acquisition pipeline. In *Computer graphics forum* (Vol. 21, pp. 149–172).
- Boschin, F., & Crezzini, J. (2012). Morphometrical analysis on cut marks using a 3D digital microscope. *International Journal of Osteoarchaeology*, 22(5), 549–562.
- Boschin, F., Zanolli, C., Bernardini, F., Princivale, F., & Tuniz, C. (2015). A look from the inside: MicroCT analysis of burned bones. *Ethnobiology Letters*, 6(2), 258–266.
- Bräuer, G., Groden, C., Gröning, F., Kroll, A., Kupczik, K., Mbua, E., . . . Schieman, T. (2004). Virtual study of the endocranial morphology of the matrix-filled cranium from Eliye Springs, Kenya. *The Anatomical Record Part A: Discoveries in Molecular, Cellular, and Evolutionary Biology*, 276(2), 113–133.
- Bretzke, K., & Conard, N. J. (2012). Evaluating morphological variability in lithic assemblages using 3D models of stone artifacts. *Journal of Archaeological Science*, 39(12), 3741–3749.
- Bruno, F., Bruno, S., De Sensi, G., Luchi, M.-L., Mancuso, S., & Muzzupappa, M. (2010). From 3D reconstruction to virtual reality: A complete methodology for digital archaeological exhibition. *Journal of Cultural Heritage*, 11(1), 42–49.
- Buzug, T. M. (2011). Computed tomography. In *Springer Handbook of Medical Technology* (pp. 311–342). Springer, New York.
- Carleo, G., Cirac, I., Cranmer, K., Daudet, L., Schuld, M., Tishby, N., . . . Zdeborová, L. (2019). Machine learning and the physical sciences. *Reviews of Modern Physics*, 91(4), 045002.
- Clarkson, C. (2013). Measuring core reduction using 3d flake scar density: A test case of changing core reduction at Klasies River Mouth, South Africa. *Journal of Archaeological Science*, 40(12), 4348–4357.
- Clarkson, C., Shipton, C., & Weisler, M. (2014). Determining the reduction sequence of hawaiian quadrangular adzes using 3D approaches: A case study from Moloka'i. *Journal of Archaeological Science*, 49, 361–371.
- Conroy, G. C., & Vannier, M. W. (1984). Noninvasive three-dimensional computer imaging of matrix-filled fossil skulls by high-resolution computed tomography. *Science*, 226(4673), 456–458.
- Conroy, G. C., Vannier, M. W., & Tobias, P. V. (1990). Endocranial features of *Australopithecus africanus* revealed by 2- and 3-D computed tomography. *Science*, 247(4944), 838–841.

- Conroy, G. C., Weber, G. W., Seidler, H., Recheis, W., Zur Nedden, D., & Mariam, J. H. (2000). Endocranial capacity of the bodo cranium determined from three-dimensional computed tomography. *American Journal of Physical Anthropology*, *113*(1), 111–118.
- Conroy, G. C., Weber, G. W., Seidler, H., Tobias, P. V., Kane, A., & Brunson, B. (1998). Endocranial capacity in an early hominid cranium from Sterkfontein, South Africa. *Science*, *280*(5370), 1730–1731.
- Courtenay, L. A., Yravedra, J., Huguet, R., Ollé, A., Aramendi, J., Maté-González, M. Á., & González-Aguilera, D. (2019). New taphonomic advances in 3D digital microscopy: A morphological characterisation of trampling marks. *Quaternary International*, *517*, 55–66.
- Courtenay, L. A., Yravedra, J., Maté-González, M. Á., Aramendi, J., & González-Aguilera, D. (2019). 3D analysis of cut marks using a new geometric morphometric methodological approach. *Archaeological and Anthropological Sciences*, *11*(2), 651–665.
- Delpiano, D., Peresani, M., & Pastoors, A. (2017). The contribution of 3D visual technology to the study of Palaeolithic knapped stones based on refitting. *Digital Applications in Archaeology and Cultural Heritage*, *4*, 28–38.
- Dennis, L. M. (2020). Digital archaeological ethics: Successes and failures in disciplinary attention. *Journal of Computer Applications in Archaeology*, *3*(1).
- Douglass, M., Kuhnel, D., Magnani, M., Hittner, L., Chodoronek, M., & Porter, S. (2017). Community outreach, digital heritage and private collections: A case study from the North American Great Plains. *World Archaeology*, *49*(5), 623–638.
- Evelyn-Wright, S., Dickinson, A., & Zakrzewski, S. (2020). Getting to grips with 3D printed bones: Using 3D models as 'diagrams' to improve accessibility of palaeopathological data. *Papers from the Institute of Archaeology*, *29*(1), 1–10.
- Evin, A., Souter, T., Hulme-Beaman, A., Ameen, C., Allen, R., Viacava, P., . . . Dobney, K. (2016). The use of close-range photogrammetry in zooarchaeology: Creating accurate 3D models of wolf crania to study dog domestication. *Journal of Archaeological Science: Reports*, *9*, 87–93.
- Frischer, B., & Dakouri-Hild, A. (2008). *Beyond illustration: 2D and 3D digital technologies as tools for discovery in archaeology*. Oxford, UK: Archaeopress.
- Göldner, D., Karakostis, F. A., & Falcucci, A. (2022). Practical and technical aspects for the 3d scanning of lithic artefacts using micro-computed tomography techniques and laser light scanners for subsequent geometric morphometric analysis. introducing the styrostone protocol. *PLoS one*, *17*(4), e0267163.
- González, M. Á. M., Yravedra, J., González-Aguilera, D., Palomeque-González, J. F., & Domínguez-Rodrigo, M. (2015). Micro-photogrammetric characterization of cut marks on bones. *Journal of Archaeological Science*, *62*, 128–142.
- Grosman, L., Smikt, O., & Smilansky, U. (2008). On the application of 3-D scanning technology for the documentation and typology of lithic artifacts. *Journal of Archaeological Science*, *35*(12), 3101–3110.
- Gümrükçü, M., & Pante, M. C. (2018). Assessing the effects of fluvial abrasion on bone surface modifications using high-resolution 3-D scanning. *Journal of Archaeological Science: Reports*, *21*, 208–221.
- Gunz, P., Mitteroecker, P., Neubauer, S., Weber, G. W., & Bookstein, F. L. (2009). Principles for the virtual reconstruction of hominin crania. *Journal of Human Evolution*, *57*(1), 48–62.
- Hassett, B. R. (2018). Which bone to pick: Creation, curation, and dissemination of online 3D

- digital bioarchaeological data. *Archaeologies*, 14(2), 231–249.
- He, D.-C., & Wang, L. (1991). Texture features based on texture spectrum. *Pattern Recognition*, 24(5), 391–399.
- Hermon, S., Polig, M., Driessen, J., Jans, G., & Bretschneider, J. (2018). An integrated 3D shape analysis and scientific visualization approach to the study of a Late Bronze Age unique stone object from Pyla-Kokkinokremos, Cyprus. *Digital Applications in Archaeology and Cultural Heritage*, 10, e00075.
- Hirst, C. S., White, S., & Smith, S. E. (2018). Standardisation in 3D geometric morphometrics: Ethics, ownership, and methods. *Archaeologies*, 14(2), 272–298.
- Hörr, C. (2009). *Considerations on technical sketch generation from 3D scanned cultural heritage*. Deutsche Nationalbibliothek.
- Jani, G., Johnson, A., Parekh, U., Thompson, T., & Pandey, A. (2020). Effective approaches to three-dimensional digital reconstruction of fragmented human skeletal remains using laser surface scanning. *Forensic Science International: Synergy*, 2, 215–223.
- Jordan, M. I., & Mitchell, T. M. (2015). Machine learning: Trends, perspectives, and prospects. *Science*, 349(6245), 255–260.
- Jurda, M., & Urbanová, P. (2016). Three-dimensional documentation of Dolní Věstonice skeletal remains: Can photogrammetry substitute laser scanning? *Anthropologie*, 54(2), 109–118.
- Kikuchi, T., & Ogihara, N. (2013). Computerized assembly of neurocranial fragments based on surface extrapolation. *Anthropological Science*, 121(2), 115–122.
- Kingsland, K. (2020). Comparative analysis of digital photogrammetry software for cultural heritage. *Digital Applications in Archaeology and Cultural Heritage*, 18, e00157.
- Knigge, R. P., McNulty, K. P., Oh, H., Hardin, A. M., Leary, E. V., Duren, D. L., ... Sherwood, R. J. (2021). Geometric morphometric analysis of growth patterns among facial types. *American Journal of Orthodontics and Dentofacial Orthopedics*, 160(3), 430–441.
- Knigge, R. P., Tocheri, M. W., Orr, C. M., & McNulty, K. P. (2015). Three-dimensional geometric morphometric analysis of talar morphology in extant gorilla taxa from highland and lowland habitats. *The Anatomical Record*, 298(1), 277–290.
- Knyaz, V., & Gaboutchian, A. (2021). Automated morphometric analysis of 3D data in paleoanthropological research. *Nanobiotechnology Reports*, 16(5), 668–675.
- Kuzminsky, S. C., & Gardiner, M. S. (2012). Three-dimensional laser scanning: Potential uses for museum conservation and scientific research. *Journal of Archaeological Science*, 39(8), 2744–2751.
- Lalondrelle, S., Sohaib, S., Castellano, I., Mears, D., Huddart, R., & Khoo, V. (2012). Investigating the relationship between virtual cystoscopy image quality and CT slice thickness. *The British Journal of Radiology*, 85(1016), 1112–1117.
- Lauria, G., Sineo, L., & Ficarra, S. (2022). A detailed method for creating digital 3D models of human crania: An example of close-range photogrammetry based on the use of Structure-from-motion (SfM) in virtual anthropology. *Archaeological and Anthropological Sciences*, 14(3), 1–13.
- Lewis, D. (2019). The fight for control over virtual fossils. *Nature*, 567(7746), 20–23.
- Linder, W. (2016). *Digital photogrammetry: A practical course* (4th ed.). Springer, Berlin.
- López-Cisneros, P., Linares-Matás, G., Yravedra, J., Maté-González, M. Á., Estaca-Gómez, V., Mora, R., ... Aguilera, D. G. (2019). Applying new technologies to the taphonomic study of La Lluera (Asturias, Spain). geometric morphometrics and the study of bone surface

- modifications (BSM). *Quaternary International*, 517, 107–117.
- Lorensen, W. E., & Cline, H. E. (1987). Marching cubes: A high resolution 3D surface construction algorithm. *ACM siggraph computer graphics*, 21(4), 163–169.
- Lovejoy, C. O., Suwa, G., Spurlock, L., Asfaw, B., & White, T. D. (2009). The pelvis and femur of *Ardipithecus ramidus*: The emergence of upright walking. *Science*, 326(5949), 71–71e6.
- Mafart, B., Guipert, G., De Lumley, M.-A., & Subsol, G. (2004). Three-dimensional computer imaging of hominid fossils: A new step in human evolution studies. *Journal of the Canadian Association of Radiologists*, 55(4), 264–270.
- Magnani, M. (2014). Three-dimensional alternatives to lithic illustration. *Advances in Archaeological Practice*, 2(4), 285–297.
- Magnani, M., Douglass, M., Schroder, W., Reeves, J., & Braun, D. R. (2020). The digital revolution to come: Photogrammetry in archaeological practice. *American Antiquity*, 85(4), 737–760.
- Martisius, N. L., McPherron, S. P., Schulz-Kornas, E., Soressi, M., & Steele, T. E. (2020). A method for the taphonomic assessment of bone tools using 3D surface texture analysis of bone microtopography. *Archaeological and Anthropological Sciences*, 12(10), 1–16.
- Massey, J. S. (2018). *Pattern of cranial ontogeny in populations of Gorilla and Pan* (Unpublished doctoral dissertation). University of Minnesota, Minneapolis, Minnesota.
- Maté-González, M. Á., Aramendi, J., Yravedra, J., Blasco, R., Rosell, J., González-Aguilera, D., & Domínguez-Rodrigo, M. (2017). Assessment of statistical agreement of three techniques for the study of cut marks: 3D digital microscope, laser scanning confocal microscopy and micro-photogrammetry. *Journal of Microscopy*, 267(3), 356–370.
- Maté-González, M. Á., Courtenay, L. A., Aramendi, J., Yravedra, J., Mora, R., González-Aguilera, D., & Domínguez-Rodrigo, M. (2019). Application of geometric morphometrics to the analysis of cut mark morphology on different bones of differently sized animals. does size really matter? *Quaternary International*, 517, 33–44.
- Maté-González, M. Á., González-Aguilera, D., Linares-Matás, G., & Yravedra, J. (2019). New technologies applied to modelling taphonomic alterations. *Quaternary International*, 517, 4–15.
- McNulty, K. P. (2005). A geometric morphometric assessment of the hominoid supraorbital region: Affinities of the Eurasian Miocene hominoids *Dryopithecus*, *Graecopithecus*, and *Sivapithecus*. In *Modern Morphometrics in Physical Anthropology* (pp. 349–373). Springer, New York.
- McPherron, S. P., Gernat, T., & Hublin, J.-J. (2009). Structured light scanning for high-resolution documentation of *in situ* archaeological finds. *Journal of Archaeological Science*, 36(1), 19–24.
- Means, B. K., McCuiston, A., & Bowles, C. (2013). Virtual artifact curation of the historical past and the NextEngine desktop 3D scanner. *Technical Briefs in Historical Archaeology*, 6(1), 1–12.
- Miyata, T., Yanagawa, M., Hata, A., Honda, O., Yoshida, Y., Kikuchi, N., ... Tomiyama, N. (2020). Influence of field of view size on image quality: Ultra-high-resolution CT vs. conventional high-resolution CT. *European Radiology*, 30(6), 3324–3333.
- Niven, L., Steele, T. E., Finke, H., Gernat, T., & Hublin, J.-J. (2009). Virtual skeletons: Using a structured light scanner to create a 3D faunal comparative collection. *Journal of Archaeological Science*, 36(9), 2018–2023.

- O'Neill, R. C., Angulo-Umana, P., Calder, J., Hessburg, B., Olver, P. J., Shakiban, C., & Yezzi-Woodley, K. (2020). Computation of circular area and spherical volume invariants via boundary integrals. *SIAM Journal on Imaging Sciences*, 13(1), 53–77.
- Orlikoff, E. R., Keevil, T. L., & Pante, M. C. (2017). Quantitative analysis of the micromorphology of trampling-induced abrasion and stone tool cut marks on bone surfaces. In *Paleoanthropology Society Conference 2018*.
- Otárola-Castillo, E., Torquato, M. G., Hawkins, H. C., James, E., Harris, J. A., Marean, C. W., . . . Thompson, J. C. (2018). Differentiating between cutting actions on bone using 3D geometric morphometrics and Bayesian analyses with implications to human evolution. *Journal of Archaeological Science*, 89, 56–67.
- O'Higgins, P., Cobb, S. N., Fitton, L. C., Gröning, F., Phillips, R., Liu, J., & Fagan, M. J. (2011). Combining geometric morphometrics and functional simulation: An emerging toolkit for virtual functional analyses. *Journal of Anatomy*, 218(1), 3–15.
- Pante, M. C., Muttart, M. V., Keevil, T. L., Blumenschine, R. J., Njau, J. K., & Merritt, S. R. (2017). A new high-resolution 3-D quantitative method for identifying bone surface modifications with implications for the Early Stone Age archaeological record. *Journal of Human Evolution*, 102, 1–11.
- Papaoiannou, G., & Karabassi, E.-A. (2003). On the automatic assemblage of arbitrary broken solid artefacts. *Image and Vision Computing*, 21(5), 401–412.
- Papaoiannou, G., Karabassi, E.-A., & Theoharis, T. (2001). Virtual archaeologist: Assembling the past. *IEEE Computer Graphics and Applications*, 21(2), 53–59.
- Papaoiannou, G., Karabassi, E.-A., & Theoharis, T. (2002). Reconstruction of three-dimensional objects through matching of their parts. *IEEE Transactions on Pattern Analysis and Machine Intelligence*, 24(1), 114–124.
- Penin, X., Berge, C., & Baylac, M. (2002). Ontogenetic study of the skull in modern humans and the common chimpanzees: Neotenic hypothesis reconsidered with a tridimensional Procrustes analysis. *American Journal of Physical Anthropology*, 118(1), 50–62.
- Pletinckx, D. (2011). Virtual archaeology as an integrated preservation method. *Virtual Archaeology Review*, 2(4), 33–37.
- Ponce De León, M. S. (2002). Computerized paleoanthropology and Neanderthals: The case of Le Moustier 1. *Evolutionary Anthropology: Issues, News, and Reviews*, 11(S1), 68–72.
- Ponce De León, M. S., & Zollikofer, C. P. (1999). New evidence from Le Moustier 1: Computer-assisted reconstruction and morphometry of the skull. *The Anatomical Record*, 254(4), 474–489.
- Ponce de León, M. S., & Zollikofer, C. P. (2001). Neanderthal cranial ontogeny and its implications for late hominid diversity. *Nature*, 412(6846), 534–538.
- Porter, S. T., Roussel, M., & Soressi, M. (2016). A simple photogrammetry rig for the reliable creation of 3D artifact models in the field: Lithic examples from the Early Upper Paleolithic sequence of Les Cottés (France). *Advances in Archaeological Practice*, 4(1), 71–86.
- Porter, S. T., Roussel, M., & Soressi, M. (2019). A comparison of Châtelperronian and Protoaurignacian core technology using data derived from 3D models. *Journal of Computer Applications in Archaeology*, 2(1), 41–55.
- Quattrini, R., Pierdicca, R., Paolanti, M., Clini, P., Nespeca, R., & Frontoni, E. (2020). Digital interaction with 3D archaeological artefacts: Evaluating user's behaviours at different representation scales. *Digital Applications in Archaeology and Cultural Heritage*, 18, e00148.



- Remondino, F., & Campana, S. (2014). 3D recording and modelling in archaeology and cultural heritage. *BAR International Series*, 2598, 111–127.
- Richards-Rissetto, H., & von Schwerin, J. (2017). A catch 22 of 3D data sustainability: Lessons in 3D archaeological data management & accessibility. *Digital Applications in Archaeology and Cultural Heritage*, 6, 38–48.
- Scherf, H. (2013). Computed tomography in paleoanthropology: An overview. *Archaeological and Anthropological Sciences*, 5(3), 205–214.
- Schulz-Kornas, E., Kaiser, T. M., Calandra, I., & Winkler, D. E. (2020). A brief history of quantitative wear analyses with an appeal for a holistic view on dental wear processes. In *Mammalian Teeth — Form and Function* (pp. 44–53). Verlag Dr. Friedrich Pfeil, Munich, Germany.
- Seidler, H., Falk, D., Stringer, C., Wilfing, H., Müller, G. B., zur Nedden, D., ... Arsuaga, J.-L. (1997). A comparative study of stereolithographically modelled skulls of Petralona and Broken Hill: Implications for future studies of Middle Pleistocene hominid evolution. *Journal of Human Evolution*, 33(6), 691–703.
- Sera, T. (2021). Computed tomography. In *Transparency in Biology* (pp. 167–187). Springer, New York.
- Spoor, F., Jeffery, N., & Zonneveld, F. (2000). Using diagnostic radiology in human evolutionary studies. *The Journal of Anatomy*, 197(1), 61–76.
- Spoor, F., Wood, B., & Zonneveld, F. (1994). Implications of early hominid labyrinthine morphology for evolution of human bipedal locomotion. *Nature*, 369(6482), 645–648.
- Strait, D. S., Weber, G. W., Neubauer, S., Chalk, J., Richmond, B. G., Lucas, P. W., ... Smith, A. L. (2009). The feeding biomechanics and dietary ecology of *Australopithecus africanus*. *Proceedings of the National Academy of Sciences*, 106(7), 2124–2129.
- Tobias, P. V. (2001). Re-creating ancient hominid virtual endocasts by CT-scanning. *Clinical Anatomy*, 14(2), 134–141.
- Tucci, G., Cini, D., & Nobile, A. (2011). Effective 3D digitization of archaeological artifacts for interactive virtual museum. *International Archives of the Photogrammetry, Remote Sensing and Spatial Information Sciences*, 38(5/W16).
- Uldin, T. (2017). Virtual anthropology: A brief review of the literature and history of computed tomography. *Forensic Sciences Research*, 2(4), 165–173.
- Weber, G. W. (2014). Another link between archaeology and anthropology: Virtual anthropology. *Digital Applications in Archaeology and Cultural Heritage*, 1(1), 3–11.
- Weber, G. W., & Bookstein, F. L. (2011). *Virtual anthropology: A guide to a new interdisciplinary field*. Springer, New York.
- Weber, G. W., Bookstein, F. L., & Strait, D. S. (2011). Virtual anthropology meets biomechanics. *Journal of Biomechanics*, 44(8), 1429–1432.
- White, S., Hirst, C., & Smith, S. E. (2018). The suitability of 3D data: 3D digitisation of human remains. *Archaeologies*, 14(2), 250–271.
- White, S., Pope, M., Hillson, S., & Soligo, C. (2022). Geometric morphometric variability in the supraorbital and orbital region of Middle Pleistocene hominins: Implications for the taxonomy and evolution of later *Homo*. *Journal of Human Evolution*, 162, 103095.
- Withers, P. J., Bouman, C., Carmignato, S., Cnudde, V., Grimaldi, D., Hagen, C. K., ... Stock, S. R. (2021). X-ray computed tomography. *Nature Reviews Methods Primers*, 1(1), 1–21.
- Wrobel, G. D., Biggs, J. A., & Hair, A. L. (2019). Digital modeling for bioarchaeologists. *Ad-*

- vances in Archaeological Practice*, 7(1), 47–54.
- Wu, X., & Schepartz, L. A. (2009). Application of computed tomography in paleoanthropological research. *Progress in Natural Science*, 19(8), 913–921.
- Yezzi-Woodley, K., Calder, J., Olver, P. J., Cody, P., Huffstutler, T., Terwilliger, A., . . . Tostevin, G. (2021). The virtual goniometer: Demonstrating a new method for measuring angles on archaeological materials using fragmentary bone. *Archaeological and Anthropological Sciences*, 13(7), 1–16.
- Ynnerman, A., Rydell, T., Antoine, D., Hughes, D., Persson, A., & Ljung, P. (2016). Interactive visualization of 3D scanned mummies at public venues. *Communications of the ACM*, 59(12), 72–81.
- Younan, S., & Treadaway, C. (2015). Digital 3D models of heritage artefacts: Towards a digital dream space. *Digital Applications in Archaeology and Cultural Heritage*, 2(4), 240–247.
- Yravedra, J., Aramendi, J., Maté-González, M. Á., Austin Courtenay, L., & González-Aguilera, D. (2018). Differentiating percussion pits and carnivore tooth pits using 3D reconstructions and geometric morphometrics. *PLoS One*, 13(3), e0194324.
- Yravedra, J., Garcia-Vargas, E., Maté-González, M. Á., Aramendi, J., Palomeque-González, J. F., Valles-Iriso, J., . . . Dominguez-Rodrigo, M. (2017). The use of micro-photogrammetry and geometric morphometrics for identifying carnivore agency in bone assemblages. *Journal of Archaeological Science: Reports*, 14, 106–115.
- Zollikofer, C. P., de León, M. S. P., Lieberman, D. E., Guy, F., Pilbeam, D., Likius, A., . . . Brunet, M. (2005). Virtual cranial reconstruction of *Sahelanthropus tchadensis*. *Nature*, 434(7034), 755–759.
- Zollikofer, C. P., de León, M. S. P., Martin, R. D., & Stucki, P. (1995). Neanderthal computer skulls. *Nature*, 375(6529), 283–285.
- Zollikofer, C. P. E., Ponce De León, M. S., & Martin, R. D. (1998). Computer-assisted paleoanthropology. *Evolutionary Anthropology: Issues, News, and Reviews*, 6(2), 41–54.
- Zvietcovich, F., Navarro, L., Saldana, J., Castillo, L. J., & Castaneda, B. (2016). A novel method for estimating the complete 3D shape of pottery with axial symmetry from single potsherds based on principal component analysis. *Digital Applications in Archaeology and Cultural Heritage*, 3(2), 42–54.